Publications

8-1990

The Luminosities of Bright H N Regions in Ngc 628 and Its O Star Formation Rate

Ted von Hippel
University of Michigan

Greg Bothun
University of Michigan-Ann Arbor

Publications

8-1990

The Luminosities of Bright H N Regions in Ngc 628 and Its O Star Formation Rate

Ted von Hippel

Greg Bothun

THE LUMINOSITIES OF BRIGHT H II REGIONS IN NGC 628 AND ITS O STAR FORMATION RATE

TED VON HIPPEL AND GREG BOTHUN

Department of Astronomy, University of Michigan, Ann Arbor, Michigan 48109

Received 25 April 1989; revised 21 March 1990

ABSTRACT

Using narrow band CCD imaging we have identified 183 bright H II regions in the Sc galaxy NGC 628. These H II regions have luminosities which indicate that they are powered by young star clusters which contain ≈ 100 ionizing stars. We attempt to reproduce the H II region LF with and without models including stellar evolution. We find stellar evolution an important parameter in understanding the H II region LF and find that it allows star-forming galaxies to be more robust to star bursting episodes. Ranking the H II regions by luminosity and assuming that luminosity evolution is due to the temporal evolution of the ionizing stars allows us to crudely determine the slope of the IMF for massive stars by matching the data with O star model atmospheres. This procedure also allows us to determine the O star formation rate and therefore predict the Type II supernova rate and the numbers of Wolf–Rayet stars in NGC 628. Overall, the data are most consistent with an IMF slope in massive stars for NGC 628 that is very near the Salpeter value found for the solar neighborhood. Our model also indicates that $\approx 1\%$ of the total supply of disk H I is presently participating in active star formation.

I. INTRODUCTION

A determination of the mass function and formation rates of massive stars in external galaxies using ground-based observations is both ambiguous and difficult primarily because these young stars radiate most of their energy in the UV. Those studies of external galaxies that have been done to date (e.g., Freedman 1985; Humphreys and McElroy 1984) are, at best, consistent with extending the solar neighborhood initial mass function (IMF) slope to masses in excess of $10 \mathscr{M}_{\odot}$. Similar trends appear to exist for embedded young stars in highly obscured regions of our own galaxy (Gatley 1990) and for the ionizing stars of small Galactic H II regions (Hunter and Massey 1990). However, these studies are by no means definitive because of varying degrees of incompleteness in the massive star samples available for nearby galaxies, including our own. This incompleteness is caused both by the difficulty of determining accurate spectral types from ground-based photometry or spectroscopy and the effects of obscuration since massive stars are generally born in molecular clouds (Shu, Adams, and Lizano 1987).

To circumvent these inherent difficulties, Kennicutt (1983) employed an alternative method of deriving the star-formation rate (SFR) in massive stars by simply counting the number of Hα photons emitted by a galaxy and converting that back into Lyman continuum (L_c) photons. While this method has met with considerable success in deriving SFRs in external galaxies, it suffers from the difficulty that uncertainty in the slope of the IMF translates into a correspondingly larger uncertainty in the total SFR. To first order, the relation between Hα equivalent width (EW) and either ($U - B$) or ($B - V$) continuum color acts as a constraint on the slope of the IMF since flatter IMFs will displace galaxies toward higher EWs at a given continuum color. Again, global data on spiral galaxies (e.g., Kennicutt 1983) are consistent with a universal IMF (in massive stars) but one can easily find individual galaxies that depart significantly from these EW Hα vs continuum color relations.

In addition, variations in internal reddening in the vicinity of H II regions renders most estimates of the global SFR a lower limit and this is the most serious source of systematic error involved in the procedure. This situation does not seem to be improved by using far-infrared fluxes, as measured by IRAS, to estimate SFRs due to the two-component nature of far-infrared emission in most galaxies (e.g., Persson and Helou 1987; Buat and Deharveng 1988; Bothun, Lonsdale, and Rice 1989—but see Devereux and Young 1990 for a dissenting view).

Nonetheless, with careful integrated balmer-line luminosity measurements it is possible to approximately determine the global underlying stellar UV luminosity in a disk galaxy and thereby estimate the total high mass SFR to within a factor of 2–3. In this paper, we employ this methodology for the case of an individual galaxy by determining the luminosities of the ≈ 200 brightest H II regions and then relating, via a modeling procedure, those luminosities to the UV luminosities of individual massive stars that must power these H II regions. Using theoretical relations between UV luminosity and stellar mass then allows for an approximate determination of the IMF for massive stars. Since the O stars which power H II regions are short lived, having main-sequence lifetimes of 3–8 Myr, we present additional modeling incorporating stellar evolution to test the sensitivity of the balmer-line luminosity technique to evolution of the ionizing stellar cluster. Previous studies have not examined fully the effects of stellar evolution on the H II region luminosity function (LF) and this has important consequences for the derived star-formation history.

To study the importance of evolution of clusters which power bright H II regions this paper models the observed H II region LF with two simple but opposite assumptions:

(1) all clusters differ only in the mass of gas involved in high mass star formation and stellar evolution is not important (the zero evolution scenario), and

(2) all clusters have an identical initial state and differ only in their evolutionary states (the evolutionary scenario).

For this particular study we selected NGC 628, a nearby, face-on (to minimize reddening problems) spiral of Hubble type Sc (Sandage 1961), previously studied with photographic techniques by Kennicutt and Hodge (1980). Its proximity, $D \approx 9$ Mpc, allowed us to measure Hα luminosities for 183 H II regions. In Sec. II we described the observations, reductions and H II region detection algorithm. In

Sec. III we discuss our modeling procedure. The results and limitations of our modeling procedure are discussed in Sec. IV and our conclusions are summarized in Sec. V.

II. OBSERVATIONS AND REDUCTION

Observations through 100 Å bandpass filters of NGC 628 were obtained in 1985 October using re-imaging optics on the Palomar 1.5 m. An RCA CCD was used as the detector and the pixel scale was 1.23″ pixel^{-1}. Division by dome flats produced images which were flat to 0.5%. There was no significant fringing through these particular filters. Candidate H II regions were identified in the ON-band frame by using the GASP image-finding algorithm to locate connected pixels that were 4σ above the local background, calculated in an annulus around each candidate. This ON-band frame is shown in Fig. 1 where many H II regions are apparent. This procedure yielded 303 peaks, some of which were spurious (e.g., cosmic ray hits, hot pixels, and foreground stars). After the images were all examined by eye, the number of H II regions was culled to 195. A histogram of equivalent widths (EW) of these 195 candidate H II regions is shown in Fig. 2 where it is clear that our sample rapidly becomes incomplete below EW H$\alpha \approx 20$ Å. (A further incompleteness exists in our data and will be discussed below.) Note that this particular measure of EW is with respect to the background galaxy and is not the intrinsic EW of the individual H II region which is typically a factor of 10 higher. We thus removed the 12 objects detected below this threshold and were left with a sample of 183 H II regions.

Photometry was then performed on these objects for apertures of diameter 2, 4, and 6 pixels. The 4 pixel (5″ ≈ 220 pc) aperture data was found to have the highest signal-to-noise ratio and it contained nearly all of the light from the H II regions. The local (galaxy + sky) background was determined by placing the same aperture in the same location on the OFF-band frame. Absolute photometry was then obtained of all 183 H II regions by tracing and modeling the
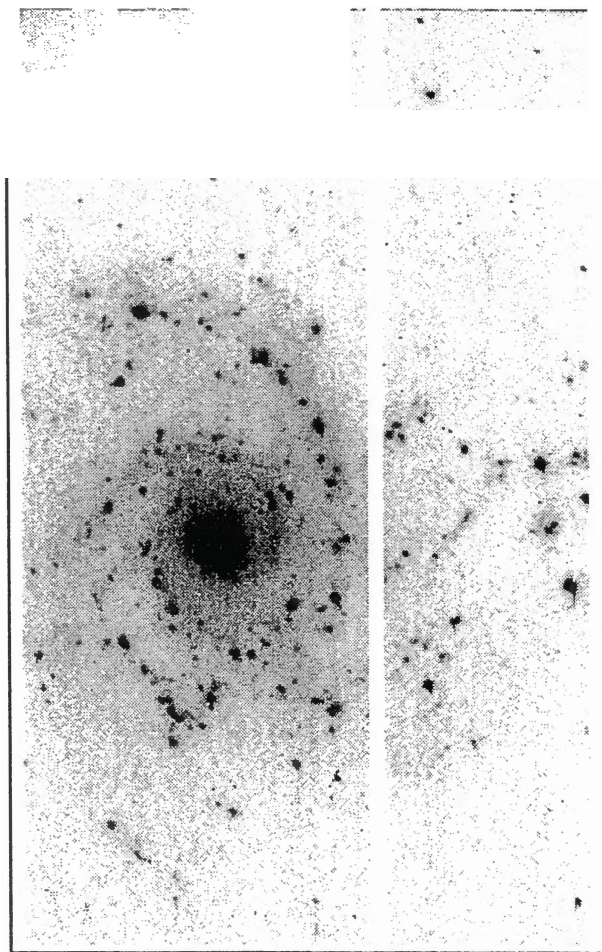
FIG. 1. NGC 628 ON-band frame. The white vertical column is a defect in the CCD which has been masked out. Note that about 20% of the area of NGC 628 is not contained in this frame. North is up and east is to the left.
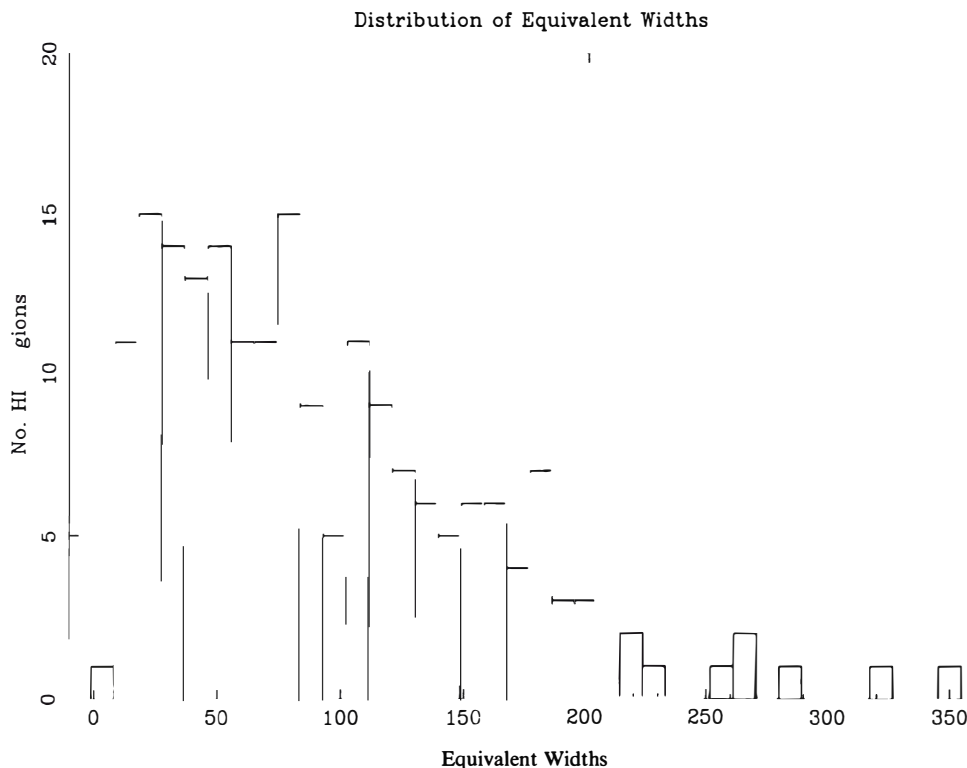
FIG. 2. Histogram of equivalent widths of Hα for 195 candidate H II regions.

responses of the filters for the recessional velocity of NGC 628 (656 km s^{-1}, Sandage and Tammann 1981) and calibrating against the average of unpublished small aperture Hα photometry obtained by Bothun, Schommer, and Kennicutt (1984) and published large aperture data of Kennicutt and Kent (1983). Our filters are sufficiently wide to contain the [N II] $\lambda\lambda$ 6548,6583 emission lines. The [N II] component was removed by assuming it contributed 33% of the total luminosity. The multiple aperture data also allowed us to determine the intrinsic EW by using annuli around each H II region to determine the background galaxy continuum level at that location. We then subtracted this value from the the continuum measured for the ionizing cluster. The residual brightness presumably represents the red continuum of the ionizing cluster itself from which we compute the intrinsic EW of each H II region.

We use a distance of 9 Mpc to NGC 628 based on a Virgocentric infall solution applied to its recessional velocity. Our derived SFR scales directly as D^2. The distribution of Hα luminosity for our sample of 183 H II regions in NGC 628 is presented in Fig. 3. These Hα luminosities are not corrected for either foreground or internal reddening. Applying the correction for foreground galactic extinction:

$A(6750) = 0.08$ mag(csc $b - 1$) (Kennicutt and Kent 1983) would only change the luminosity by 3% ($b = -45.7$ for this galaxy), so we do not make this correction. Variations in internal reddening are handled by the model, as discussed below.

As can be seen from Fig. 3, 7% of the Hα luminosity is contained in the brightest H II region, 15% in the brightest 3 H II regions, 19% in the brightest 5 H II regions, and 24% in the brightest 8 H II regions. This distribution in the bright end of the LF of NGC 628 is typical of Sc galaxies (see Kennicutt, Edgar, and Hodge 1989). The turnover at log Hα ≈ 38.3 is due to incompleteness. At our pixel resolution,

these fainter H II regions easily blend into the background and cannot be unambiguously recovered. In particular, Fig. 6 of Kennicutt (1988) shows that the mean log Hα luminosity at a diameter of 220 pc (our aperture size) is ≈38.5. In Fig. 4 we plot our derived H II region luminosities in comparison with the LF derived by Kennicutt et al. (1989) for NGC 628. We scale our data by a factor of 1.2 since our CCD frame is missing approximately 20% of the area of NGC 628 (see Fig. 1) and correct the Kennicutt et al. data to our distance of 9 Mpc. Overall the agreement is quite good for log Hα ≳ 38.3 and below that level our data becomes incomplete. This incompleteness, however, is not a serious problem for our analysis since the H II regions that we did successfully detect comprise 80% of the total Hα luminosity, and thus contain the bulk of information regarding the recent history of massive star formation in NGC 628.

III. REPRODUCING THE H II REGION LF: THE MODEL

a) Overview

The model is designed to convert observed Hα luminosity into a derived SFR and constrain the IMF. Towards this end we consider two simple, but opposite hypotheses. In the first hypothesis, the zero evolution scenario, we assume that the H II region LF in NGC 628 is due only to a range in ionizing cluster mass which we model as a power law distribution. Thus, a very luminous H II region is powered by many massive unevolved stars, whereas a less luminous H II region is powered by fewer of these stars. Further, the majority of the ionization is due to the most massive stars and after they die the cluster continues to evolve, but there may be no detectable H II region associated with it. Other possible contributors to the LF, such as stellar evolution, an IMF differing from cluster to cluster or dust variations are ignored under this assumption. Deriving a SFR then requires only a zero-

HII Region Luminosity Function
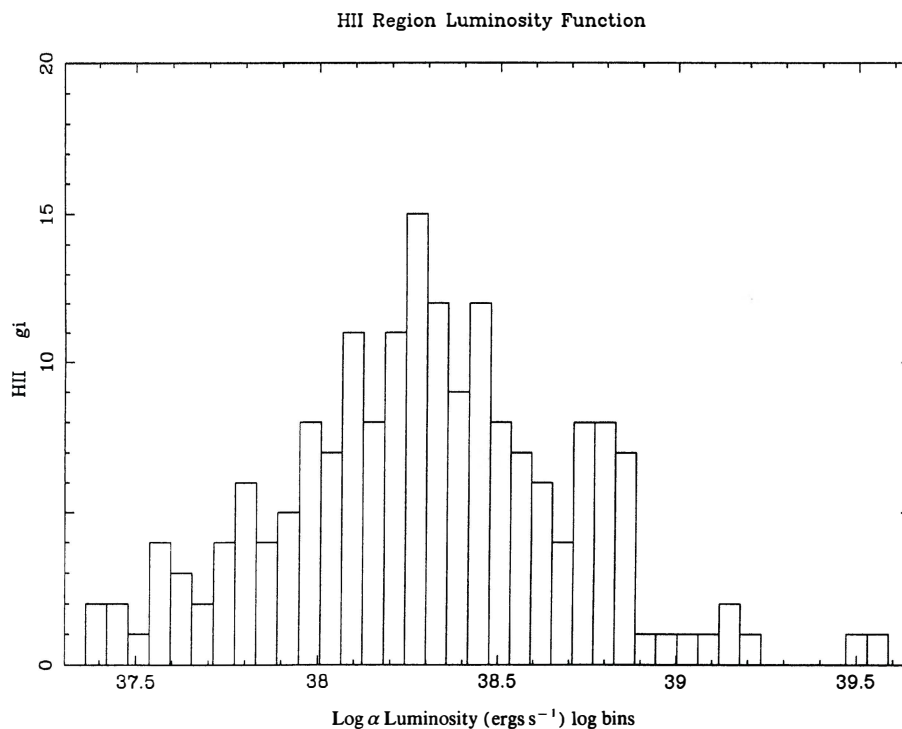
FIG. 3. Distribution of Hα luminosity for 183 H II regions.

Comparison with Kennicutt et al LF
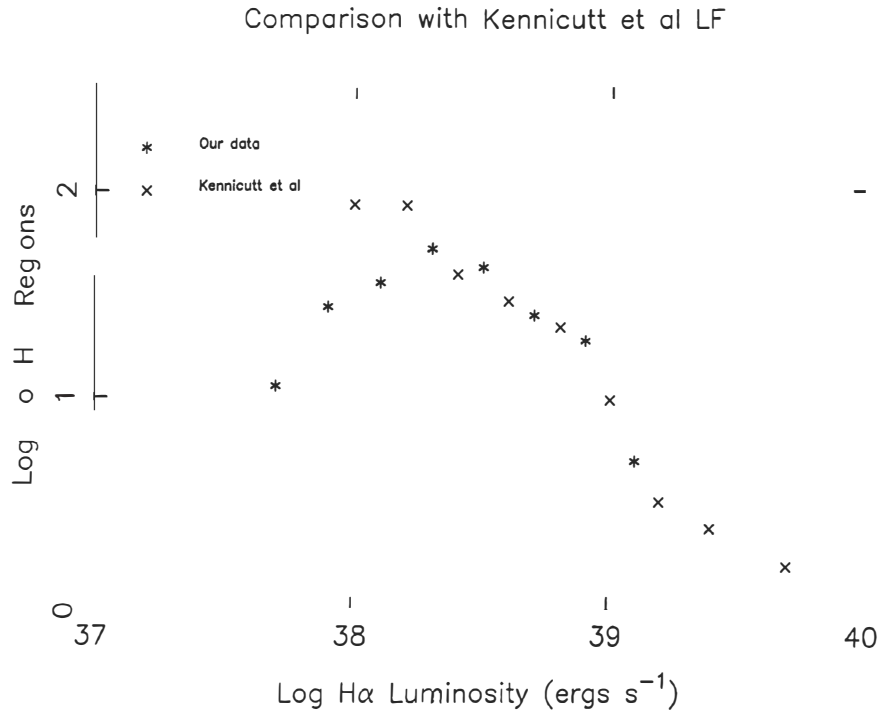
FIG. 4. Derived H II region luminosities vs Kennicutt *et al.* luminosities (see text).

age main-sequence (ZAMS) mass-UV luminosity relation. In the second hypothesis, the evolutionary scenario, we assume that stellar evolution and the disappearance of the most massive stars is the major agent which is responsible for determining the form of the H II LF in NGC 628. This evolutionary scenario requires a more elaborate mass–age–UV luminosity relation. While the zero evolution scenario has been used extensively, the evolutionary scenario has not been fully tested. Some previous studies (e.g. Kennicutt 1983) have incorporated stellar evolution up to a point by assigning lifetime-weighted luminosities to the high mass stars. These studies did not explicitly consider the case where the most massive stars have evolved off the main sequence and left the next most massive stars to power the H II regions.

The conversion of observed Hα luminosity back to the UV luminosity emitted by the embedded stars is accomplished by simple radiative transfer considerations using constraints on the stellar population via an assumed IMF. We define the IMF as $dN/dM = AM^{-\alpha}$, where $\alpha = 2.35$ is the Salpeter (1955) value. For the zero evolution scenario we build a ZAMS mass UV luminosity relation from ZAMS mass–temperature relations (Bertelli, Bressan, and Chiosi 1985; Maeder and Meynet 1987) and a temperature–UV flux relation (Mihalas 1972). For the evolutionary scenario we build a mass–age–UV luminosity relation from these same relations plus a mass–lifetime relation (Bertelli, Bressan, and Chiosi 1985; Maeder and Meynet 1987). The mass–lifetime relation yields only a mass–lifetime–UV luminosity relation, instead of a time-dependent mass–age–UV luminosity relation. Thus our models do not evolve individual stars, just as the previous studies have not, but our models do evolve the cluster as a whole by turning off stars after they leave the main sequence.

b) Details

All of our models start with a ZAMS single burst population, a given IMF power law slope ($\alpha = 1, 2,$ and 3 are used, see Figs. 6 and 7) and total mass. A surface temperature, and thereby a UV luminosity, is assigned to each star. The UV luminosity for the stellar population is then determined and stellar UV photons are converted to nebular Hα photons by the ratio of the effective Hα recombination coefficient to the case B recombination coefficient (Osterbrock 1974). This assumes that the nebula is optically thick to UV light. Additionally, absorption by dust is ignored at this point, though corrections are applied later. For a nebular temperature of 10 000 K one stellar UV photon is converted to 0.452 nebular Hα photons. This is sufficient to create a H II region LF for the zero evolution scenario. For the evolutionary scenario the population is evolved in 10^5 yr timesteps and the nebular Hα luminosity recalculated. Evolving stars is limited to turning them off after their H-burning lifetimes are exceeded. We found that the He-burning stages of stellar evolution did not contribute significantly to the total ionizing luminosity, and later stages were even less important. This is due to both the shorter timescales and generally lower surface temperatures of stars in their late evolutionary stages. The cluster evolution is followed for 10^8 yr, long after the H II regions have effectively died.

Though the detailed physics of converting stellar UV photons to nebular Hα photons is not controversial, the assumptions which allow us to quantify the underlying UV luminosity are. For the zero evolution scenario we assume:

(1) All bright H II regions have an underlying ZAMS stellar population which differs from cluster to cluster only in the amount of mass involved in high mass star formation. Bright H II regions in this context specifically mean those

H II regions typically observed in extragalactic objects, which are powered by clusters of stars rather than one or a few stars. Note that under this assumption we may miss the most massive clusters if they require dense molecular clouds for their formation.

(2) All 183 H II regions have approximately the same internal dust content and line-of-sight extinction.

For the evolutionary scenario we assume:

(1) All bright H II regions have nearly the same initial size and mass of gas associated with star formation. Specifically, all 183 H II regions are powered by an equivalent mass underlying stellar population which is observed in different evolutionary states. Under this assumption, we are implicitly assuming that young clusters may emerge from their molecular cocoons on a similar timescale and one which is substantially shorter than the lifetime of the H II region.

(2) All 183 H II regions have approximately the same internal dust content and line-of-sight extinction.

(3) All were born smoothly in time over the last 10^7 yr, and were not the result of a few, intermittent bursts of star formation.

While the assumptions of the zero evolution scenario have been explicitly used by many researchers, our evolutionary scenario is new and we therefore attempt to at least partially justify its assumptions:

(1) Temporal behavior helps to explain the observations of Kennicutt, Edgar, and Hodge (1989) and Kennicutt and Hodge (1980) that the brightest H II regions strongly prefer spiral arms and are seldom seen in the interarm region. If clusters are born in spiral arms, then stellar evolution will naturally lead to lower luminosity H II regions as they diffuse out from the spiral arm. This situation could easily occur over the $\approx 10^7$ yr lifetime of a typical H II region. Temporal behavior may further explain the distribution of hottest stars in small Galactic H II regions observed by Hunter and Massey (1990). They find the hottest star in most H II regions to be types O9–B0, with few clusters containing earlier type stars. The *hottest* cluster star only depends weakly on the slope of the IMF or the cluster mass, but strongly on cluster age.

(2) If evolution is important then Hα EWs and luminosities should correlate positively, since aging clusters produce less Hα luminosity and more red continuum from evolved stars. At the very earliest times the red continuum may oscillate considerably if it is dominated by just a few (or one) M supergiants. At later times evolved stars steadily increase the red continuum and the Hα luminosity declines due to disappearance of the hottest stars. Fig. 5 shows that the lower luminosity H II regions in NGC 628 indeed have significantly lower EW than their more luminous counterparts which implies they are more evolved. In the zero evolution scenario, all the H II regions would be expected to have the same EW.

(3) The internal dust content could vary from H II region to H II region, but would have the *same* effect on the models as variance in the mass of star-forming gas. The line-of-sight absorption is expected to be constant towards NGC 628 as it is observed face-on.

(4) A star burst hypothesis for this galaxy seems unlikely as there is no morphological organization to the location of H II regions ranked by luminosity. This test also showed no preference with radius for the most luminous H II regions (see also Hodge and Kennicutt 1983).

To implement the evolutionary model we convert the observed H II region LF into an evolutionary sequence for a "standard" H II region, simply by ranking them in luminosity. Thus lower luminosity H II regions are in more advanced evolutionary stages than their more luminous counterparts.

Luminosity versus Corrected Equivalent Width
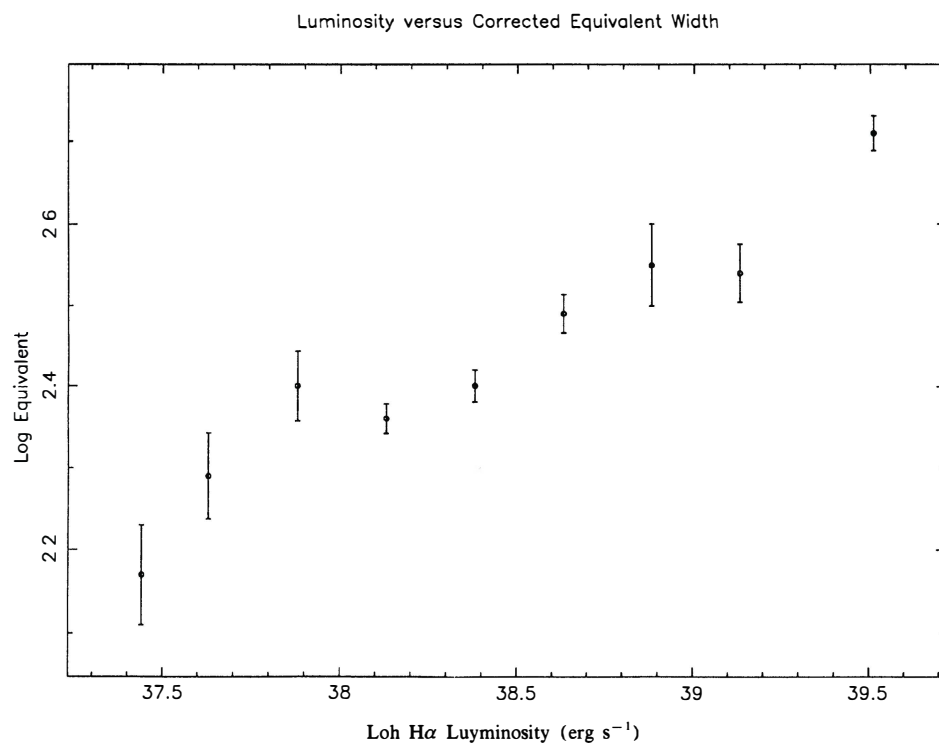
FIG. 5. Luminosity vs equivalent width for 183 H II regions binned in luminosity. Error bars represent $\sigma/\sqrt{N}$ for each bin.

Note that creating a temporal sequence of H II regions biases later, fainter evolutionary stages to be underrepresented due to incompleteness. We attempt to correct for this below. Such a ranking allows models of H II region luminosity evolution to be compared directly with the data. Alternatively, H II region luminosity evolution models could be used to fit the shape of the H II region LF, but we feel the former approach is more useful and adheres more closely to the data. The observational data ranked by luminosity are presented in Fig. 6 as " + "s. The horizontal scale is the number of H II regions brighter than a given luminosity and thus is functionally equivalent to units of time. The scaling in time is discussed in Sec.IVb.

Both the zero evolution and evolutionary scenarios are built up from stellar evolution and atmosphere models from the literature. The stellar evolution models (Bertelli, Bressan, and Chiosi 1985; Maeder and Meynet 1987) contain mass loss and overshooting and are consistent with observations (Mihalas and Binney 1981; Allen 1963). The Bertelli, Bressan, and Chiosi grid of stellar evolution models is used from 5 to 9 $\mathcal{M}_\odot$ while the Maeder and Meynet grid is used from 15 to 120 $\mathcal{M}_\odot$. The Mihalas (1972) atmospheres models are unblanketed non-LTE log g = 4 calculations. Since only UV photons ionize the nebula we determined stellar luminosity in photons with energies between 1 and 4 Ry. The adopted physical relations for both scenarios are parametrized by the values listed in Table I.

The accuracy of the adopted models are not without uncertainty. Perhaps the least certain element of either scenario is the surface temperature–UV luminosity calibration. The stellar photons which give rise to nebular balmer emission are principally those with energies between 1 and 4 Ry (228–912 Å), which resides in a currently unobserved part of the spectrum. Thus, though the model atmospheres used are the best available, they are observationally unchecked (see, however, an attempt with Voyager by Holberg et al. 1982). They are, however, consistent with other published model atmospheres (Panagia 1973 and references therein; Kurucz, Peytremann, and Avrett 1974), especially for the hottest stars. For a parametrization of stellar UV flux as a function of surface temperature see the Appendix.

Less uncertain, but also troublesome, is stellar mass loss. In principle, our cluster evolution models could recalculate the masses of the stars as they evolve, determining new surface temperatures and new UV luminosities. Such evolutionary tracks are still uncertain, however, so we constrain the total UV luminosity within reasonable limits by running the evolutionary scenario models with two different mass–surface temperature relations. The ZAMS mass–surface temperature relation provides the upper limit to UV luminosity,

and thus the lower limit to the SFR and allows direct comparison between the evolution and zero evolution scenarios. The luminosity-weighted temperature relation provides a more reasonable value for stellar UV luminosity by assigning a lifetime-integrated UV luminosity to each star. This latter relation provides $\approx 1/2$ the UV luminosity that the ZAMS relation does, and it accounts empirically for the effects of mass-loss and temperature evolution, though not for the effects of radius (e.g., log g) evolution. We believe neglect of surface gravity evolution is unimportant relative to the uncertainties in the model atmospheres. These relations are listed in Table I. The models require a very fine grid of mass, age, and temperature points, which were produced by a smooth spline of the values contained in Table I.

IV. RESULTS

a) Nonevolving Power Law Distribution of H II Region Masses

The simplest nonevolving scenario which most closely matches the observed distribution of H II region luminosities in NGC 628 is a power law distribution of masses, normalized to the log luminosity histogram (see Fig. 3). A least-squares minimization fit yields:

$$\log (\text{cluster number}) \approx - 1.0 \log (\text{cluster mass}).$$

This value is typical for Sc galaxies (Kennicutt et al. 1989). The model fits can be seen in Fig. 6(a)–6(c), where the " + "s are our data and the line is the model for an IMF slope of 1 (panel a), 2 (panel b), and 3 (panel c). Though the fit to the data was done with a smooth distribution of masses the model luminosities are not smooth due to both integer stars and some numerical noise. Regardless, the general shape of the zero evolution models fit the data well, at least for luminosities $\geqslant \log L = 38.3$, where our observations begin to become incomplete. Clearly, in the zero-evolution case, little constraint on the IMF is available. This is not surprising because of the greater flexibility allowed by identifying the distribution of ionizing cluster masses as the dominate parameter.

Table II summarizes the numbers and total masses of O stars in NGC 628 required by our zero evolution models in the case of one magnitude of internal extinction. The numbers and masses of OB stars are calculated by assuming a single slope power law down to 5 $\mathcal{M}_\odot$. The fits of Figs. 6(a)–6(c) require 2200–5400 O stars for NGC 628, or 12–30 O stars per H II region, with the total mass in these stars ranging from 1.2–1.8 × 10⁵ $\mathcal{M}_\odot$, depending on the adopted IMF slope. The mass of gas converted to stars greater than 5 $\mathcal{M}_\odot$ (B6) ranges from 1.4–9.3 × 10⁵ 5 $\mathcal{M}_\odot$. If the cluster

TABLE I. Stellar parameter relations.

Mass ($M_\odot$)	Lifetime (yr)	T_{surf} (INT) (K)	Flux[a] (INT)	T_{surf} (ZAMS) K	Flux[a] (INT)
5.0	1.2036×10^8	15 136	1.07×10^{18}	17 378	3.14×10^{18}
9.0	3.4851×10^7	21 380	4.57×10^{19}	23 988	3.33×10^{20}
15.0	1.2105×10^7	29 904	2.51×10^{22}	31 477	6.73×10^{22}
20.0	8.8064×10^6	33 575	2.14×10^{23}	35 645	5.52×10^{23}
25.0	7.0887×10^6	35 908	6.13×10^{23}	38 726	1.56×10^{24}
40.0	4.7912×10^6	39 527	1.91×10^{24}	44 875	3.93×10^{24}
60.0	3.7108×10^6	40 971	2.56×10^{24}	49 317	4.62×10^{24}
85.0	3.3245×10^6	42 313	3.13×10^{24}	52 481	5.89×10^{24}
120.0	2.9379×10^6	44 410	3.82×10^{24}	54 828	9.31×10^{24}

[a] Flux in 1 to 4 Ry photons at the star's surface cm^{-2} s^{-1}.
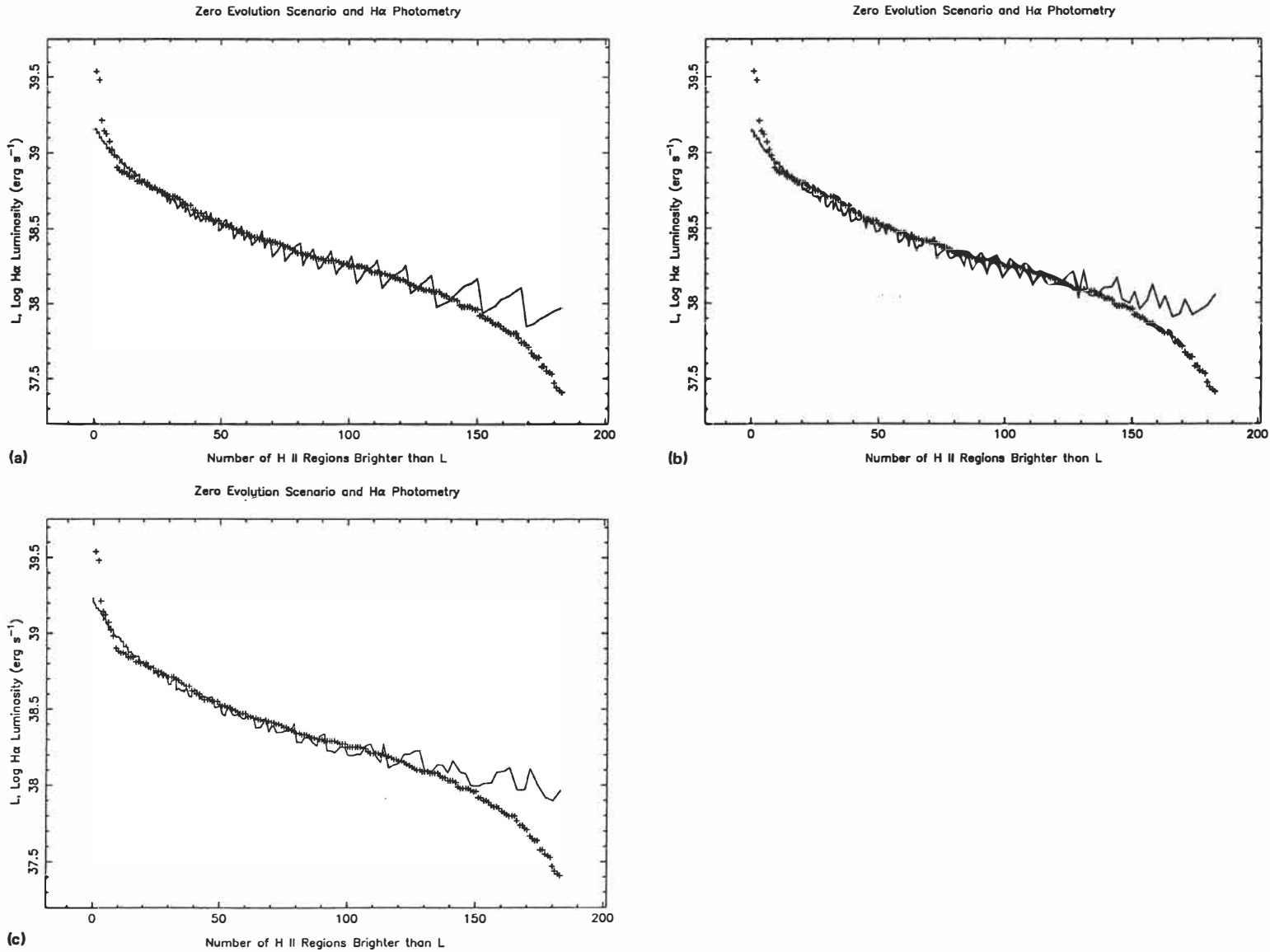
FIG. 6. Best-fit zero evolution models to the observed H II region luminosities. The " + " symbols are our data, and the lines our models for the IMF power law slope of 1 (a), 2 (b) and 3 (c).

TABLE II. Population statistics for zero evolution scenario.

No. of Stars		Mass($M_\odot$)	In stars	
O	OB	O	OB	Notes[a,b]
2200	3 900	1.2×10^5	1.4×10^5	$\alpha = 1$, Fig. 6(a)
3400	15 900	1.4×10^5	2.5×10^5	$\alpha = 2$, Fig. 6(b)
5400	99 500	1.8×10^5	9.3×10^5	$\alpha = 3$, Fig. 6(c)

[a] All of these models run with 1.0 mag internal extinction at Hα.
[b] Statistics for all of NGC 628, not an individual H II region.

power law is extrapolated down to the luminosity of Orion (5×10^{36} erg s^{-1}, Hunter and Massey 1990) there should be 300 Orions in NGC 628.

A timescale can be tentatively introduced to the zero evolution scenario by assuming that no two H II regions can have their luminosities differ appreciably due to evolution (the importance of which is shown in the next section). This implies all H II regions are within 3×10^6 yr of each other in age, at the maximum (see Fig. 7). If the H II regions are not hosting single-burst ZAMS populations, then the maximum age spread is probably no more than $\approx 10^6$ yr for the zero evolution scenario to be valid. This yields a high mass SFR $\approx 4 \times 10^{-3}$ O stars yr^{-1} and a H II region birthrate in NGC 628 of $\approx 2 \times 10^{-4}$ H II regions yr^{-1}. Extrapolation a single power law IMF down to 0.1 $5 \mathcal{M}_\odot$ and assuming a star-formation efficiency of 10% (an intermediate value from Shu, Adams, and Lizano 1987), would then imply a few $\times 10^6$-$\approx 10^9 \mathcal{M}_\odot$ of gas participating in star formation in NGC 628.

b) An Evolving Standard H II Region

The evolutionary models are fit to the observations through a least-squares minimization procedure. The fit using the ZAMS mass-surface tennperature calibration, which provides a lower limit to the SFR, is shown in Figs. 7(a)–7(c). The more realistic luminosity-weighted mass-surface temperature calibration is shown in Figs. 7(d)–(f). In these figures, the models are computed with 1.0 mag of internal extinction (cf. Kennicutt 1983). Figure 8 shows the effect of varying degrees of extinction on the models. The steplike behavior of the models is real and is caused by the death of individual stars.

The match of models and observation in these figures is somewhat artificial. Though there are few free parameters which affect a fit in the vertical direction, the horizontal scale of the photometric observations have no known time dependence. They were compressed linearly, over the observed luminosity range, to fit the theoretical curves. Observations of other galaxies that might offer a larger dynamic range in H II region luminosity could potentially reveal a mismatch between the photometry and the theoretical curves, and force adjustment of the timescale imposed on the photometry. It should be noted, however, that the photometry covers 2 orders of magnitude in luminosity and contains 80% of the total Hα luminosity emitted by NGC 628, so a significant re-adjustment seems unlikely. But our main point is that regardless of how the data falls off at lower light levels, and even regardless of the three assumptions made for the evolutionary scenario, a rough fit between the models and the overall *level* of the photometry must yield the underlying

stellar population that provides the UV luminosity. The major uncertainties imposed by the horizontal compression are uncertainties in the timescale.

With respect to the model fits, the maximum flexibility available in this realm is no more than about a factor of 1.5, even if one were to choose an IMF power law with a slope as steep as 3. Incompleteness in our LF does affect the times-cales, however, becoming important for times greater than 6×10^6 yr. A complete LF down to log $L \approx 37$ would contain more faint H II regions, and thus yield a data curve stretched toward longer times at lower luminosities. Wherever the timescales are used to derive a SFR this effect is unimportant. This is because adding fainter H II regions serves to simultaneously increase the number of newly formed stars and lengthen the timescales in our model, thus conserving our derived, time-averaged, SFR.

Taking the match between observations and theory at face value, the curves cannot be made to match before about 3×10^6 yr, the lifetime of the most massive star produced in these populations, $\approx 100 \mathcal{M}_\odot$. At these earliest times the evolutionary scenario is equivalent to the zero evolution scenario because of the single-burst population assumption and because our models do not follow the evolution of individual stars across the main sequence. In the OB mass range, the most massive stars live out much of their lives before the less massive stars can evolve onto the main sequence (Yorke 1986; Mihalas and Binney 1981, and references therein), bringing into question the single-burst population concept. We thus also ran models with stars born randomly over a few $\times 10^6$ yr. These continuous-burst models showed better fit to the data at early times, without much changing the quantitative results derived from the single-burst models, which we adhere to for the remainder of the discussion.

The maximum timescale over which the photometry could be fit to the models is set by the shape of the theoretical curves. Our models indicate these H II regions are all powered by larger star clusters (≈ 100 ionizing stars—see below) and that stars less massive than 20 $\mathcal{M}_\odot$ (B stars) are incapable of powering H II regions at the luminosities which we observe. Note that in models with less than 20 to 40 O stars, the H II region is essentially ionized by the single most massive star since it provides the same UV luminosity as the rest of the stellar population.

The best match between the shape of the thoretical curves and the entire set of observations requires an IMF with a slope of ≈ 2, as displayed in Figs. 7(a)–7(f). Regardless of how we set the temporal scale for the data, we cannot match an IMF slope as steep as 3 and we have even greater difficulty with slopes as shallow as 1. Since there are only eight of the very brightest H II regions yielding the upper part of the observational curve, we sought also a best fit by excluding them since these brightest H II regions possibly are overly massive, and are not our "standard" H II regions, though they are not larger than the other H II regions as judged by the form of their aperture–magnitude relation. The general results were little affected by removing the brightest eight H II regions, except that the remaining data is best fit by a steeper IMF slope of ≈ 3. As expected, models with somewhat less mass in star-forming gas gave better fits to this dataset, but the differences were not great. The choice of best IMF depends very little on the horizontal scale used for the data, but is applicable only to stars with lifetimes less than about 9×10^6 yr. This corresponds to stars more massive than $20 \mathcal{M}_\odot$ (an O9 star, Maeder and Meynet 1987).
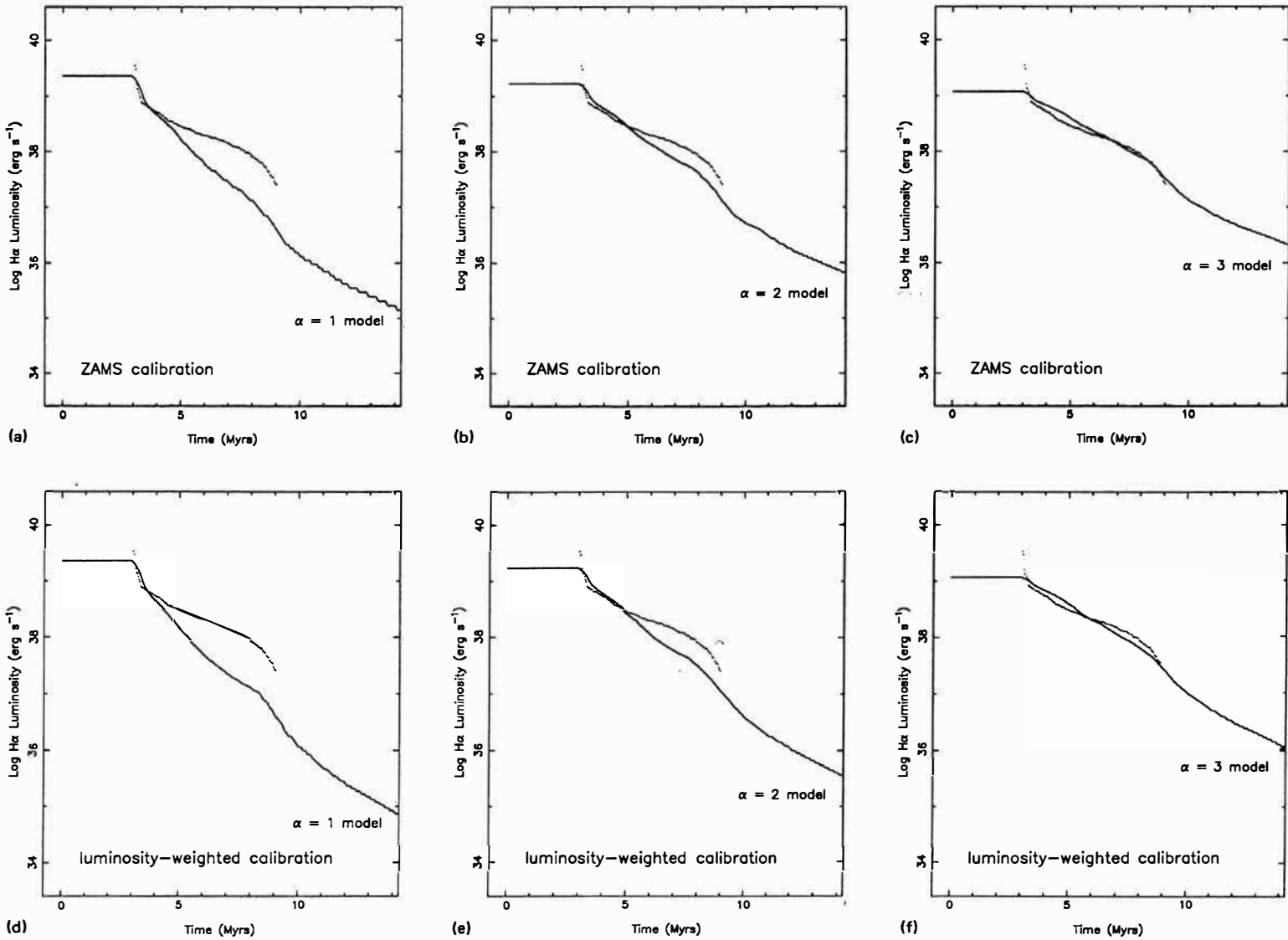
FIG. 7. Best-fit evolution models to the observed H II region luminosities. (a)–(c) detail models with the ZAMS calibration, while (d)–(f) detail models from the luminosity-weighted calibration. The models displayed are for an IMF power law slope of 1 [(a) and (d)], 2 [(b) and (e)], and 3 [(c) and (f)].

Effect of Extinction on Models
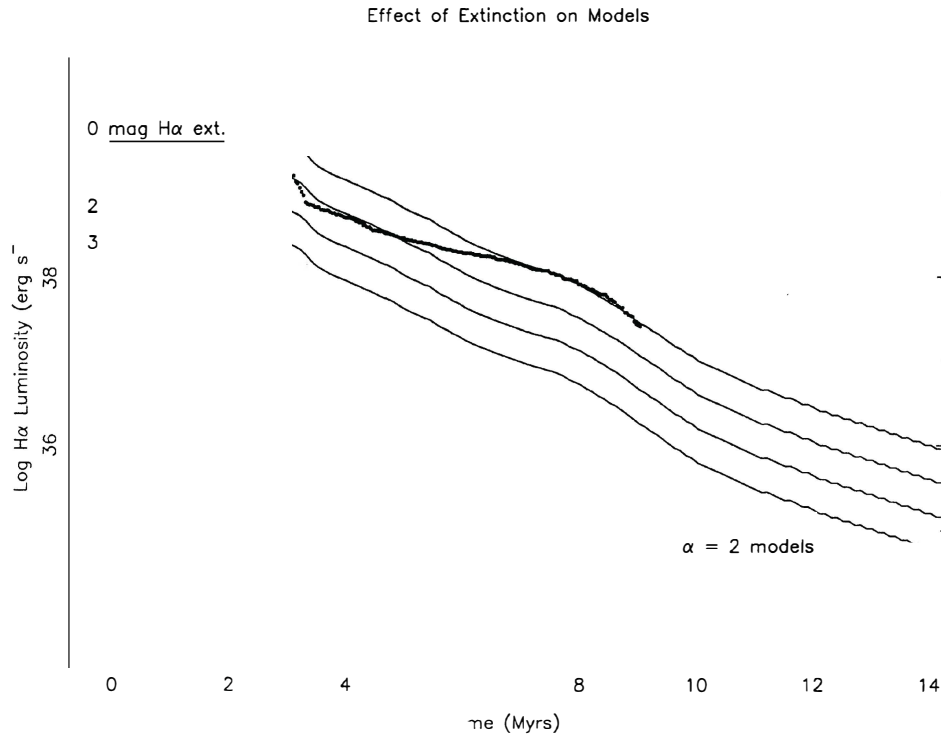
FIG. 8. The effect of varying degrees of extinction on the models. The models exhibites here are identical to Fig. 7(d) (our best fit), but with 0, 1, 2, and 3 mag of extinction at Hα.

The models of Fig. 7 may be vertically rescaled by two means. The mass of star-forming gas may be adjusted, or the magnitudes of extinction due to dust may be varied. Table III summarizes the numbers of O stars and their total mass, that can be derived from our models in the case of one magnitude of internal extinction; the reader can adjust the SFR upwards to match higher extinction estimates. The fits of Figs. 7(a)–7(c) (the ZAMS calibration) require 50–113 O stars per H II region, with the total mass in these stars ranging from 2750–4760 $\mathscr{M}_\odot$, depending on the adopted IMF slope. The mass of gas converted to stars greater than 5$\mathscr{M}_\odot$ (B6) ranges from 3130–18 890 $\mathscr{M}_\odot$. This model underestimates the O star count per H II region because of the ZAMS mass-surface temperature calibration.

The fits of Figs. 7(d)–7(f) (the luminosity-weighted temperature calibration) require 89–240 O stars, with the total mass in O stars ranging from 5020 to 9310 $\mathscr{M}_\odot$. The mass of gas converted to stars greater than 5$\mathscr{M}_\odot$ is 5760–39 360 $\mathscr{M}_\odot$ Extrapolating these fits down to 0.1$\mathscr{M}_\odot$ with a single power law IMF yields $\approx 7200 \mathscr{M}_\odot$ ($\alpha = 1$), $3.3 \times 10^4 \mathscr{M}_\odot$ ($\alpha = 2$), and $3.1 \times 10^6 \mathscr{M}_\odot$ ($\alpha = 3$) of gas-forming stars in each of these H II regions. Assuming a star-formation efficiency of 10%, there are 1.3×10^7–$5.7 \times 10^9 \mathscr{M}_\odot$ of gas participating in star formation in NGC 628. The upper limit in this range can be excluded by simple arguments involving gas depletion timescales in a disk galaxy. The $\alpha = 2$ case, which we have previously argued provides a reasonable fit to the data, has $6.0 \times 10^7 \mathscr{M}_\odot$ of gas participating in star formation and this represents $\approx 1\%$ of the total supply of disk H I in NGC 628. If this SFR were to sustain itself over the next 10^9 yr, the available gas supply in NGC 628 would be entirely depleted.

We can make a number of additional predictions regarding high mass stars in NGC 628. A limit may be put on the age of H II regions and thereby their birth rate can be determined. Our observations yielded 183 objects with ages less than 9×10^6 yr, for a birth rate of 2.0×10^{-5} H II regions yr^{-1}. This, coupled with our best estimate of the number of O stars per H II region (≈ 210 for $\alpha = 2$), yields a SFR of 4.3×10^{-3} O stars yr^{-1} or a total of 19 000 O stars currently on the main sequence. Since each of these stars is expected to result in a supernova explosion, our timescales also yield a predicted supernova rate. Extrapolating the IMFs used to lower masses, and using a lower mass cutoff of 8$\mathscr{M}_\odot$ for the production of supernovae (Yorke 1986) each H II region should produce ≈ 600 ($\alpha = 2$) stars that will eventually explode. This leads to a Type II supernovae rate of 1.2×10^{-2} supernovae yr^{-1}. Additionally, 80 ($\alpha = 2$) stars per H II region will be produced which are massive enough to pass through the Wolf–Rayet (WR) phase (40$\mathscr{M}_\odot$ limit; Maeder and Meynet 1987). The WR phase lasts about 5×10^5 yr and thus we expect ≈ 800 ($\alpha = 2$) WR stars, at any given time, in NGC 628. The number of stars which will experience a WR phase and the number which will explode in a Type II supernova outburst are also listed in Table III.

Both the evolution and zero evolution scenarios give approximately the same SFR and gas depletion timescales since the fewer O stars required per H II region in the zero evolution scenario is balanced by the shorter lifetimes of these H II regions. The evolutionary scenario predicts ≈ 5 times as many O stars per currently observable H II region and ≈ 10 times as much gas involved in O star production per H II region. The relative difference in the ratio of star counts to mass is caused by the large number ($\approx 1/2$) of the O stars which already have evolved off the main sequence in the evolutionary scenario. Averaged over a suitably long time (e.g., 10^9 yr), both scenarios, of course, produce the same number of O stars. The major difference is that the

TABLE III. Population statistics for standard H II region.

| No. of Stars | | | | Mass ($M_\odot$) | In stars | |
O	OB	SN	WR	O	OB	Notes[a,b]
84	151	128	52	4760	5 460	$\alpha = 1$, all, Fig. 7(a)
100	489	288	41	4310	7 860	$\alpha = 2$, all, Fig. 7(b)
113	2011	752	26	3860	18 890	$\alpha = 3$, all, Fig. 7(c)
50	86	72	30	2750	3 130	$\alpha = 1$, cul
61	305	180	26	2660	4 900	$\alpha = 2$, cul
75	1384	517	17	2550	12 930	$\alpha = 3$, cul
165	310	259	103	9310	10 870	$\alpha = 1$, all, Fig. 7(d)
207	1012	599	78	8780	16 169	$\alpha = 2$, all, Fig. 7(e)
240	4184	1567	51	8110	39 360	$\alpha = 3$, all, Fig. 7(f)
89	159	135	55	5020	5 760	$\alpha = 1$, cul
129	643	380	52	5540	19 269	$\alpha = 2$, cul
170	2994	1120	37	5740	28 130	$\alpha = 3$, cul

[a] All of these models run with 1.0m ag internal extinction at Hα.
[b] cul = without eight brightest HII regions.

evolutionary model allows H II regions to be observable for a longer period of time as they can continue to be ionized by stars as late as O9–B0 (see also Hunter and Massey 1990). This necessarily requires the ionizing cluster to be more massive than in the zero evolution case where one assumes that the lifetime of the observable H II region is essentially that of the most massive star in the ionizing cluster. By requiring H II regions to be essentially coeval, the zero evolution scenario, in principle would allow observers to find disk galaxies without any H II regions, unless they are turning on and off in a relatively steady state. The evolutionary scenario, in contrast, is at least twice as robust to star-formation histories which may be bursty or episodic in nature.

V. SUMMARY

We have used narrowband Hα imaging of the face-on Sc spiral NGC 628 to identify bright (H$\alpha \geqslant 10^{38}$ ergs^{-1}) H II regions and to measure their luminosities. A total of 183 H II regions with Hα + [N II] equivalent widths $\geqslant 20$ Å (relative to the background light of the galaxy) were detected by our procedure. We have sought to use these data to test the importance of stellar evolution to the H II region LF. Theoretically, evolution is expected to influence the total UV luminosity emitted by the embedded clusters since bright H II regions are powered predominantly by short-lived stars. Observationally, Kennicutt, Edgar, and Hodge (1989) and Kennicutt and Hodge (1980) have noted the tendency of brightest H II regions to strongly prefer spiral arms over interarm regions, which we attribute to cluster evolution since the arm crossing time is similar to O star lifetimes. Additionally, Hunter and Massey (1990) found the distribution of hottest stars in small Galactic H II regions to peak at types O9–B0, as expected for clusters in later evolutionary states.

We have attempted to reproduce the observed Hα LF with both a power law distribution of cluster masses and no stellar evolution and with a single "standard" H II region (no mass or dust variation) with stellar evolution. Although *both* methods can fit the data, there are a number of important physical differences between these two approaches:

(1) Models including evolution allow a rough determination of the IMF slope, whereas models without evolution are largely insensitive to the IMF slope because of the considerable freedom to arbitrarily choose ionizing cluster masses.

Thus our comments regarding IMF constraints are only valid if stellar evolution is indeed the dominant factor which determines the form of the H II region LF.

(2) The derived H II region lifetimes and birthrates, and the number of O stars currently on the main sequence, depend heavily on the role of stellar evolution in the clusters which power these regions. In this way, star burst events which occur on a timescale of $\approx 10^7$ yr can leave their imprint in the resultant H II region LF.

Under the assumption that the form of this observed LF is entirely due to the evolution of a "standard" H II region powered by a cluster of stars, the evolutionary model constrains both the O star-formation rate and the IMF associated with star formation.

Our model is a general one and can be applied to any galaxy where an H II region LF is measured. Applying this technique to the specific case of NGC 628 yields the following results:

(3) A *lower* limit of 50–110 O stars are powering or were powering (many have evolved) each bright H II region, with the total mass in these stars ranging from 2600 to 4800 $\mathcal{M}_\odot$.

(4) The typical bright H II region is most likely initially powered by 90–240 O stars, with the total mass in these stars ranging from 5000 to 9300 $\mathcal{M}_\odot$. To the extent that stellar populations can be characterized by a single power law IMF, our models indicate a best fit for a slope which is very similar to the Salpeter value of 2.35. A value of $\alpha = 2$ yields $\approx 3 \times 10^4 \mathcal{M}_\odot$ of gas-forming stars in each of these H II regions. Slopes as steep as 3 can be ruled out on the basis of gas consumption arguments while slopes as shallow as 1 do not provide a good fit to the bulk of the data.

(5) The H II regions are less than 10^7 yr old, and have a birth rate of $\approx 2 \times 10^{-5}$ H II regions yr^{-1}. This yields an O star formation rate of $\approx 4 \times 10^{-3}$ stars yr^{-1} which in turn implies that there are a total of 19 000 O stars that are currently on the main sequence in NGC 628.

(6) If these O stars go through a Wolf–Rayet evolutionary phase and terminate their lifetimes as Type II supernovae, then we predict a supernova rate of $\approx 1 \times 10^{-2}$ supernovae yr^{-1}, and a population of ≈ 800 Wolf–Rayet stars.

(7) When combined with a reasonable value for the efficiency of star formation (e.g., 10%), our model indicates that approximately 1% of the total supply of disk gas is participating in current star formation as manifested by massive stars. This is a rather small amount but it is easily sufficient to power the H II regions at their observed level and hence to illuminate the spiral pattern in NGC 628. In this respect, such a spiral pattern would seem to be a rather ethereal component of disk galaxies which will cease to be illuminated by O stars in another 10^9 yr if the current SFR is maintained.

APPENDIX

Mihalas (1972) provides log $g = 4$, NLTE OB model atmospheres from 15 000 to 55 000 K for which we summed the flux in 1 to 4 Hydberg photons. The log of the flux in these ultraviolet photons is plotted against effective surface temperature $\times 10^{-3}$ K. We found this could be parametrized by a fourth order equation rather well, and did this by

UV Flux for Mihalas Log g = 4 NLTE Model Atmospheres
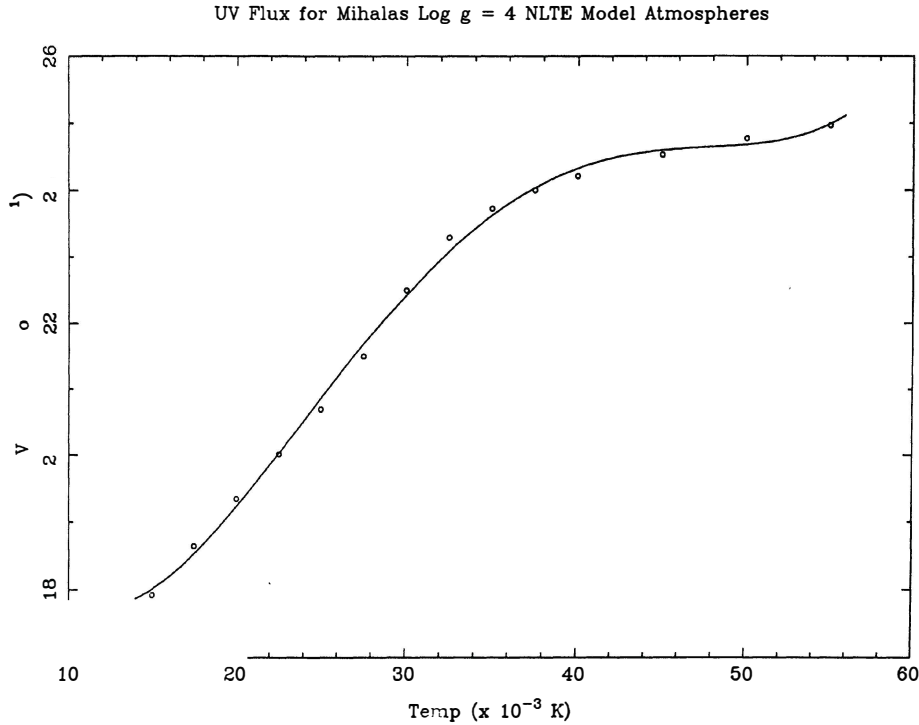
FIG. 9. Parametrization of Mihalas (1972) log g = 4 NLTE model atmospheres. The circles are the sum of 1 to 4 Rydberg photons $cm^{-2} s^{-1}$ at the star's surface. The smooth curve is our 4th order fit to these points.

a least squares minimization procedure. This parametrization is the smooth curve plotted in Fig. 9, and is as follows: $\log(uv\,\text{flux}) = a + bt + ct^2 + dt^3 + et^4$, where $t =$ (effective surface temperature)$/1000.0$, $a = 24.3885$,

$b = -1.32018$, $c = 8.289\,881e\text{-}2$, $d = -1.7313e\text{-}3$, and $e = 1.207427e\text{-}5$.

We caution that this parametrization should only be used within Mihalas's temperature range 15 000–55 000 K.

REFERENCES

Allen, C.W. (1963). *Astrophysical Quantities* (William Clowes and Sons, Ltd., London).

Bertelli, G., Bressan, A.G., and Chiosi, C. (1985). Astron. Astrophys. **150**, 33.

Bothun, G.D., Lonsdale, C.J., and Rice, W. (1989). Astrophys. J. (submitted).

Buat, V., and Deharveng, J.M. (1988). Astron. Astrophys. **195**, 60.

Devereux, N.A., and Young, J.S. (1990). Astrophys. J. Lett. **350**, L25.

Freedman, W.L. (1985). Astrophys. J. **299**, 74.

Gatley, I. (1990). Preprint.

Hodge, P.W., and Kennicutt, R.C. (1983). Astrophys. J. **267**, 563.

Holberg, J.B., Forrester, W.T., Shiemansky, D.E., and Barry, D.C. (1982). Astrophys. J. **257**, 656.

Humphreys, R.M., and McElroy, D.B. (1984). Astrophys. J. **284**, 565.

Hunter, D.A., and Massey, P. (1990). Astron. J. **99**, 846.

Kennicutt, R.C. (1983). Astrophys. J. **272**, 54.

Kennicutt, R.C. (1988). Astrophys. J. **334**, 144.

Kennicutt, R.C., Edgar, B.K., and Hodge, P.W. (1989). Astrophys. J. **337**, 761.

Kennicutt, R.C., and Hodge, P.W. (1980). Astrophys. J. **241**, 573.

Kennicutt, R.C., and Kent, S.M. (1983). Astron. J. **88**, 1094.

Kurucz, R. L., Peytremann, E., and Avrett, E. H. (1974). *Blanketed Model Atmospheres for Early-Type Stars* (Smithsonian Institution, Washington, DC).

Maeder, A., and Meynet, G. (1987). Astron. Astrophys. **182**, 243.

Mihalas, D. (1972). NCAR-TN/STR-76.

Mihalas, D., and Binney, J. (1981). *Galactic Astronomy: Structure and Kinematics* (W.H. Freeman and Co., San Francisco).

Osterbrock, D.E. (1974). *Astrophysics of Gaseous Nebulae* (W.H. Freeman and Co., San Francisco).

Panagia, N. (1973). Astron. J. **78**, 929.

Persson, C.J.L., and Helou, G. (1987). Astrophys. J. **314**, 513.

Salpeter, E.E. (1955). Astrophys. J. **121**, 161.

Sandage, A. (1961). *The Hubble Atlas of Galaxies*, Publ. No. 618 (Carnegie Institute of Washington, Washington, DC).

Sandage, A., and Tammann, G.A. (1981). *A Revised Shapley-Ames Catalog of Bright Galaxies*, Publ. No. 635 (Carnegie Institute of Washington, Washington, DC).

Shu, F.H., Adams, F.C., and Lizano, S. (1987). Annu. Rev. Astron. Astrophys. **25**, 23.

Yorke, H.W. (1986). Annu. Rev. Astron. Astrophys. **24**, 49.